www.cadanda.com
Computer-Aided Design AND APPLICATIONS

Preliminary Shape Similarity Analysis and Standardization for Pre-Bent Rod Design for Adult Spinal Deformity Correction

Ayane Soutome[1], Satoshi Kanai[2], Hiroaki Date[3], Terufumi Kokabu[4], Yuichiro Abe[5], Hiroshi Moridaira[6], Hiroshi Taneichi[7], and Hideki Sudo[8]

[1]Hokkaido University, bvsb_0410@eis.hokudai.ac.jp
[2]Hokkaido University, kanai@ssi.ist.hokudai.ac.jp
[3]Hokkaido University, hdate@ssi.ist.hokudai.ac.jp
[4]Hokkaido University, m990015jp@yahoo.co.jp
[5]Eniwa Hospital, menchi@athena.ocn.ne.jp
[6]Dokkyo Medical University, morihey@dokkyomed.ac.jp
[7]Dokkyo Medical University, tane@dokkyomed.ac.jp
[8]Hokkaido University, hidekisudo@yahoo.co.jp

Corresponding author: Kanai Satoshi, kanai@ssi.ist.hokudai.ac.jp

Abstract: Spinal deformity is a disease that causes a three-dimensional deformation of the spinal column. When it worsens, surgery is required to screw correction rods to the spinal column. However, the surgery requires intraoperative rod bending work, which burdens the patients and causes unexpected rod breakage inside the body. Therefore, "pre-bent" rods comprising several rods with standardized shapes have been proposed to solve these problems. When designing pre-bent rods, knowing the number of rods to be prepared and the kinds of shapes required is essential. In this paper, we propose a geometric processing technique to identify an optimal set of these standardized pre-bent rod shapes for surgeries on adult spinal deformity and describe the similarity evaluation among existing rod shapes using CT scan, medial axis extraction, and iterative closest point algorithm. Moreover, we present the derivation of standardized rod shapes using hierarchical cluster analysis and the best fit of the B-spline curve to each cluster. Finally, we discuss the effectiveness of pre-bent rod shapes derived from CT scans of 26 existing rods of 13 patients.

Keywords: Shape similarity, shape standardization, point clouds, iterative closest points, medial axis, pre-bent spinal rods, spinal deformity, hierarchical cluster analysis, CT scan, point cloud registration.
DOI: https://doi.org/10.14733/cadaps.2023.797-813

1 INTRODUCTION

Spinal deformity is a common disorder that causes an unnatural three-dimensional (3D) deformation of the spinal column (Figure 1(a)). Although new, less-invasive surgical options, such as vertebral

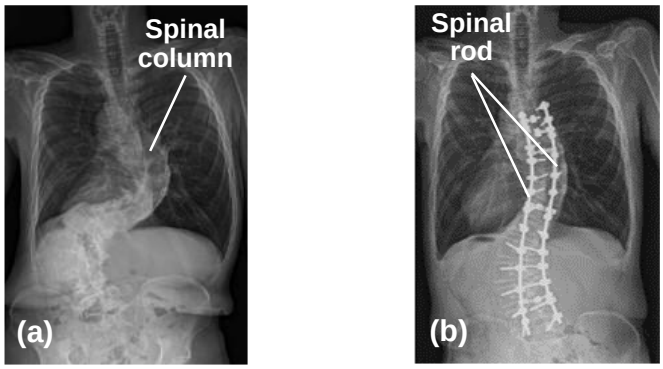

Figure 1: (a) Spinal deformity and (b) two spinal rods implanted by correction surgery.

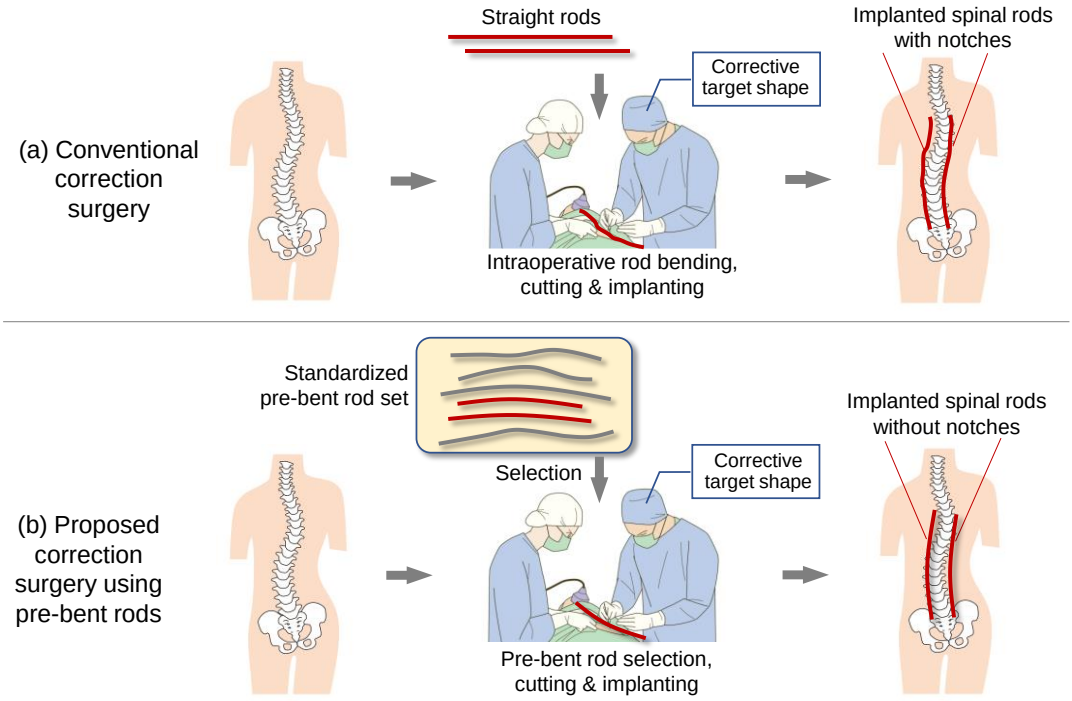

Figure 2: (a) Conventional correction surgery and (b) proposed correction surgery using pre-bent rods.

body tethering, have been introduced for early-onset scoliosis [23], posterior spinal fusion with posterior instrumentation is currently the gold standard for treating adolescent idiopathic scoliosis to restore sagittal and coronal contours [22]. During surgery, two metal rods called "spinal rods" are screwed to the spinal column's left and right sides (Figure 1(b)). The rod curvature significantly influences postoperative thoracic kyphosis [28]. Currently, orthodontic surgeons manually bend the straight rods during surgery to fit the corrective target shape of the thoracic curve suitable for each patient (Figure 2(a)). However, since the bending accuracy significantly depends on the surgeons' experience, this intraoperative rod bending work raises the patient's burden due to the increase in surgery time [17]. In addition, if the bent shape of the rod does not match the deformity, it will cause excessive stress to the patient's spine and spinal rods. Moreover, rod breakage inside the body will increase due to notched damages caused by the bending work [20].

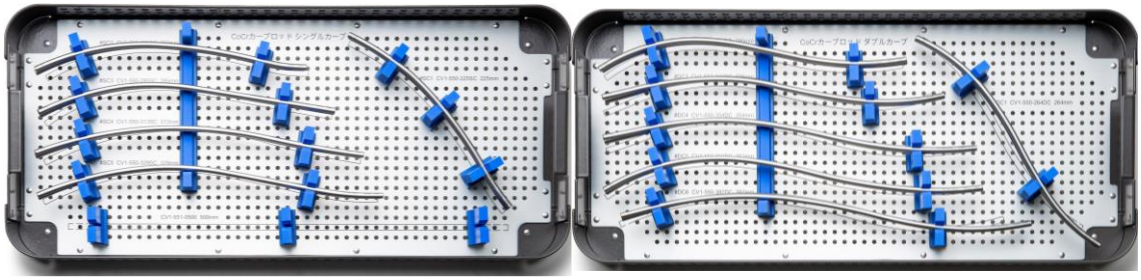

Figure 3: A set of standardized pre-bent rods for idiopathic scoliosis.

To solve the above problem, the authors proposed a surgical operation method for spinal deformity correction that uses a set of pre-bent rods [17, 31–32] (Figure 2(b)). The pre-bent rods are manufactured from straight round steel bars using a dedicated mechanical fixture. Therefore, the swept surface can represent the geometry of a pre-bent rod along a path defined by a 2D or 3D smooth free-form curve. The pre-bent rods comprise several standardized rods that have already been bent and deformed during manufacture, and a rod that best suits a patient's spine is selected from the standardized rods during surgery (Figure 3). This method does not require any bending operation during surgery and thus can reduce the patient's burden and risk of breakage. When designing pre-bent rods, the number of rods to be prepared and the kind of shapes required must be known.

To design the pre-bent rods for adolescent idiopathic scoliosis in [17], the authors first made a manually traced drawing of the spinal rods during surgery. Next, they manually fit 2D lines and circles to the traced rod contours on a two-dimensional (2D) CAD system. Subsequently, from a large collection of these 2D CAD data of the rod contours, they analyzed the similarity in spinal rods of different shapes used in recent idiopathic scoliosis surgeries. Thus, they showed that preparing 10 standardized rods whose center curves are expressed by 2D planar curves is sufficient [17] (Figure 3). Due to our surgical technique being performed without reference to the intraoperative coronal alignment of the adolescent idiopathic scoliosis deformity, there was no relationship between the shape of the rods and scoliosis classification, such as Lenke classification.

Conversely, the deformity patterns in adult spinal deformity patients are geometrically complicated compared to those in adolescent idiopathic scoliosis patients. Therefore, the pre-bent rods whose center curves are expressed by 2D planar curves designed for idiopathic scoliosis surgery cannot be used for adult spinal deformity. Instead, pre-bent rods whose center curves are designed with 3D spatial curves are required for correction surgeries of adult spinal deformity. When rod center curve shapes are 3D, the rod shape cannot be measured by manual tracing and fitting 2D lines and circles to the rod contours and center curves. Moreover, the 3D similarity between the rod shapes must be evaluated, and standardized 3D pre-bent rod shapes must be identified based on the similarity analysis.

In this paper, we propose a method to identify an optimal set of standardized 3D pre-bent rod shapes for correction surgeries of adult spinal deformities. For this purpose, we measured the existing spinal rod shapes using a medical CT scan to extract the rods' center points from the measurements. Subsequently, we analyzed the 3D similarity between the center curves of the rods and derived an optimal set of standardized pre-bent rod shapes whose center curves are represented by 3D spatial curves. The proposed method can be considered an extension of our former study [17] to 3D. However, this study addressed all issues related to rod measurement, similarity assessment, and standardized shape derivation caused by the extension to 3D.

The latter part of the paper is organized as follows. In Section 2, related works are reviewed, and issues and solutions are clarified. In Section 3, the geometric processing for the shape similarity analysis and standardization of pre-bent rods' shapes are detailed. In Section 4, a case study result is shown. Finally, in Section 5, the conclusion and future work are presented.

2 RELATED WORK

From a geometric modeling aspect, this study mainly comprises three techniques: (1) evaluating the similarity among rods having free-form shapes, (2) clustering multiple rod shapes based on the similarity measures, and (3) finding an optimized rod shape that represents a set of rod shapes included in each cluster. The related works on these techniques are introduced, and we clarify the issues these techniques pose when they are applied to identifying an optimal set of standardized 3D pre-bent rod shapes for correction surgeries.

2.1 Similarity Measures between Curves

So far, there has been considerable research on shape similarity measures in 3D computer vision and geometric modeling. They have been applied to shape retrieval, shape comparison, and shape matching problems, and many similarity metrics have been proposed for those purposes. Most of them aimed to quantify the differences between 3D surfaces, meshes, and solid shapes. The review papers by Cardone et al. [5], Iyer et al. [15] and Santini et al. [29] summarized these metrics adequately. For example, Fu et al. [11] proposed an integrated approach based on the integration of Gaussian curvature to develop similarity measures between two free-form surfaces. Surazhsky et al. [33] created a shape matching technique between two free-form surfaces using unit normal fields of two surfaces for the similarity measure between surfaces. Sahillioğlu [27] recently presented an exhaustive survey on the recent advances in 3D shape correspondence techniques and the similarity measures used in them. In Sahillioğlu [27], the registration-based approach is regarded as one of the effective ways to find the correspondence between two free-form shapes under a non-rigid deformation and to evaluate the similarity measure between them from a degree of deformation, such as in [8],[9]. However, these techniques require costly computation and must solve non-rigid registration problems that include complex optimization or parameterization. Furthermore, they assume a relatively large difference between two shapes, such as non-rigid deformation, and their similarity measures do not quantify a difference in shapes in a geometrically intuitive manner. Therefore, the similarity measures based on sophisticated non-rigid registration are unsuitable for our study.

Similarity measures have also been proposed for quantifying the difference between 2D shapes. For example, Kuragano et al. [18] utilized the distributions and radius of curvature along a B-spline curve for the similarity measure of curves. They defined the similarity between two curves by taking the dot product of the discretized distributions and radius of curvature of two curves. Lee et al. [19] proposed a similarity measure between 2D polygonal curves using Fourier descriptors and applied it to vertebral image retrieval. Ramanathan [25] proposed a matching and retrieval of 2D shapes bounded by free-form curves using a medial axis transformation, evaluating an L2 distance between the statistical signatures of two axes as the similarity measure. Guo et al. [12] evaluated the geometric similarity between 2D polygonal shapes using Freeman chain code and fuzzy matching, further applying it to solve the problem of 2D free-form shape layout.

As a simple but efficient approach, Zhang [37] proposed iterative point matching, such as iterative closest points (ICP) [4], for registering two free-form curves. In their matching, the weighted mean-squared distance between the closest points sampled on two curves was used as a dissimilarity measure between two curve shapes.

Due to the registration using ICP, this weighted mean-squared distance between curves adopted in [37] can be regarded as the dissimilarity measure invariant to the 3D transformation of curves. Additionally, this measure is easy to implement and can intuitively quantify the average distance between two free-form curves. Therefore, we use the root-mean-square (RMS) distance between the closest points sampled on two center curves of the rods as a dissimilarity measure between two existing rods in our study.

2.2 Curve Shape Clustering

Several techniques have been proposed to cluster curve shapes based on similarity measures. Recently, in statistics and data mining, sophisticated curve clustering and curve registration algorithms have been actively studied and have been applied to problems in medicine, business, socioeconomics, and engineering [1, 6–7, 21]. According to Jacques et al. [16], clustering approaches fall within four classes: raw-data clustering, filtering methods, adaptive methods, and distance-based methods. The distance-based curve clustering approach is based on dissimilarity or distance measures between curves.

However, these curve clustering techniques mainly focus on clustering the time-series data, including relatively large noises, and they primarily aim to estimate statistical models behind curves. Conversely, in our problem setting, the shapes of rod center curves are smooth, bounded, noiseless, and not significantly dissimilar. Moreover, when pre-bent rods are implanted into a patient's spine in surgery, the distance between the selected rod shapes and the corrective target shape of the thoracic curve should not exceed the maximum tolerance allowed for the treatment. Therefore, we chose a conventional hierarchical clustering technique [26] to find optimal clusters of existing rod shapes. In hierarchical clustering, we can use the mean-squared distance as a dissimilarity measure of rod shapes and specify the maximum distance tolerance allowed for the treatment. Moreover, we can easily find the other optimal clusters of the rods when changing the tolerance value.

2.3 Finding the Representative Curve Shape for a Cluster

Once the optimal clusters of rod shapes are found, we need to find an optimized rod shape representing the multiple rod shapes included in a cluster. Recently, statistical shape models (SSM) have been actively studied in 2D and 3D medical model-based image segmentation. Constructing an SSM comprises extracting the mean shape and several variation modes from a collection of training samples [14]. SSMs are actively used for bone [13], [30], brain [35], and heart [3] image segmentation tasks, among others. Mesh-, point-, and volume-based SSMs have been actively studied.

The mean shape of SSM can be regarded as a shape representing a collection of geometries included in the training samples. Recently, Zhang et al. [36] constructed the SSM of femurs from existing bones and optimized the orthopedic plate shape using the parametrization of the abutted surface based on the mean shape of the SSM. In addition, Engelborghs et al. [10] indicated that the SSM of the population could be effectively used to design an orthopedic implant shape that obtains a better fit while maximizing population coverage.

However, to construct an SSM, we need atomic landmark-based 3D non-rigid registration among homologous sample shapes and dimensionality reduction of the training set through principal component analysis. The construction is generally time-consuming, laborious, and error-prone.

In our problem setting, the rods' center curves can be expressed by a collection of 3D free-form curves, and the positions and orientations of the center curve shapes in a cluster are already best aligned with each other in a cluster using ICP. Moreover, the difference in shape and length among the center curves in a cluster is relatively small. Therefore, we first sample a dense point cloud on the center curve of each rod included in a cluster. Afterward, we find a 3D free-form curve that best fits the dense points on all center curves in a least-squares manner, and we adopt the curve as a representative curve shape for a rod cluster. This method is fast, easy to implement, and can work well if the difference in the curve length contained in a cluster remains relatively small.

3 METHOD OF SHAPE SIMILARITY ANALYSIS AND STANDARDIZATION OF PRE-BENT RODS

3.1 Outline and Range of Analysis

Figure 4 shows the outline of the proposed method's process pipeline, which comprises the following processes:

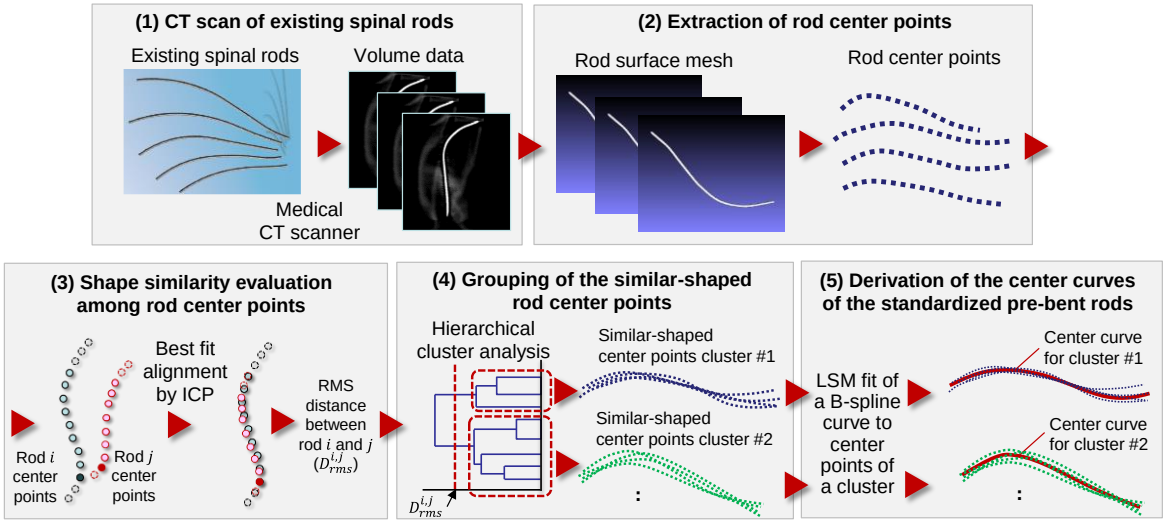

Figure 4: Process pipeline of existing rod shape similarity analysis and standardization of pre-bent rod shapes.

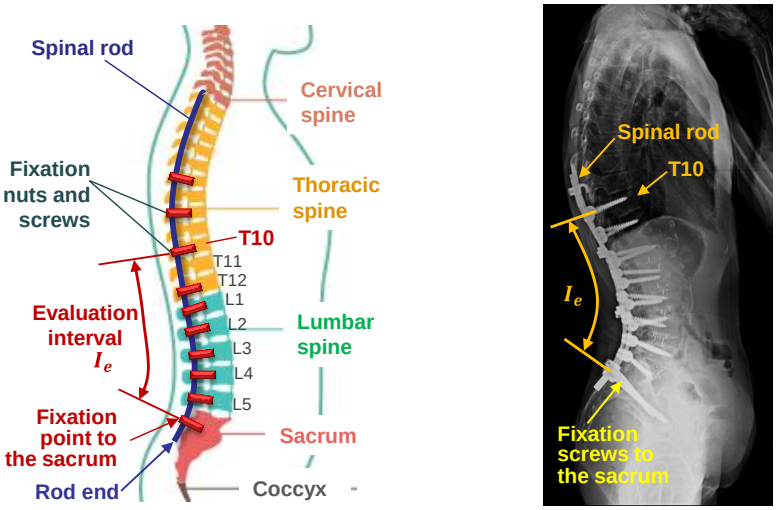

(a) Evaluation interval (b) A radiography example

Figure 5: Similarity evaluation interval I_e of spinal rods.

(1) A CT scan of existing spinal rods used in past corrective surgeries
(2) Extraction of the rods' center points from the CT scan by mesh processing
(3) Shape similarity evaluation of rod center point sets using ICP [4]

(4) Grouping of similar-shaped rod center points through hierarchical cluster analysis to identify the number of pre-bent rods
(5) Derivation of the center curves of each standardized pre-bent rod by the least-square fitting of a B-spline curve with similar-shaped center points
(6) Generation of standardized rods' surfaces

The details of the processes are described in Sections 3.2 to 3.5.

The shapes of the spinal rods for adult spinal deformity correction exhibit moderate differences among patients in the interval from the sacrum to the lumbar spine and to the thoracic spine T10

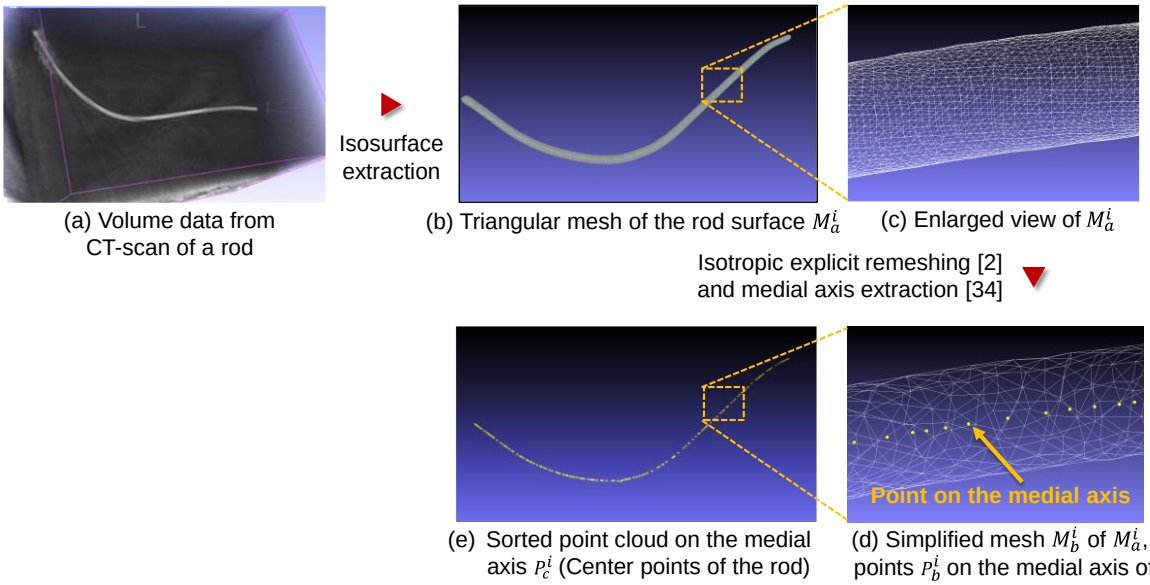

Figure 6: Process of the extraction of rod center points from CT-scan.

(Figure 5). Most rod breakages also occur within this interval due to intraoperative bending. Conversely, the similarity among the rods becomes significantly low in patients from the distal part of the center of their thoracic spine. Moreover, standardizing the rod shape in the distal part is difficult, and rod breakage rarely occurs in this part. For these reasons, the similarity evaluation and standardization of rod shapes were limited to the evaluation interval I_e between the sacrum and the thoracic spine T10 (Figure 5). In addition, since the reference point at surgery is always taken at the rod's fixation point to the sacrum, we place the starting point of the interval I_e at the fixation point and evaluate the similarity between existing rod shapes so that the starting point of I_e always coincides.

3.2 CT scan of Existing Spinal Rods and Extraction of Rod Center Points

The center curve of a spinal rod for adult spinal deformity correction often exhibits a spatial curve shape, and the existing rod shape cannot be measured by manual tracing. Therefore, in our method, the rods are measured three-dimensionally with a medical CT scanner (image resolution 512 × 512 pixels) immediately after being bent during surgery. Afterward, the rod surface M_a^i, represented by a triangular mesh, is extracted from the CT volume data as the isosurface (Figure 6(a), 6(b), and 6(c)).

Next, to stabilize the extraction of rod center points from the rod surface, M_a^i is first re-meshed using isotropic explicit re-meshing [2] to generate a simplified mesh M_b^i with an edge length of about 1 mm. Subsequently, iterative mesh contraction and topological simplification [34] are applied to

M_b^i to derive a dense point cloud P_b^i sampled on the medial axis of M_b^i (Figure 6(d)). The points in the point cloud P_b^i are then sorted so that the two closest points lie next to each other. This sorted point cloud P_c^i is finally treated as the center points of rod i (Figure 6(e)).

3.3 Shape Similarity Evaluation among Rod Center Points

Next, shape similarity in the evaluation interval I_e is evaluated for the center points of all existing rods. Thus, best fit alignment is first performed by ICP [4] between every pair of the center points $\langle P_c^i, P_c^j \rangle$ of rod $i(\in R)$ and $j(\in R)$ included in the CT-scanned rod set R.

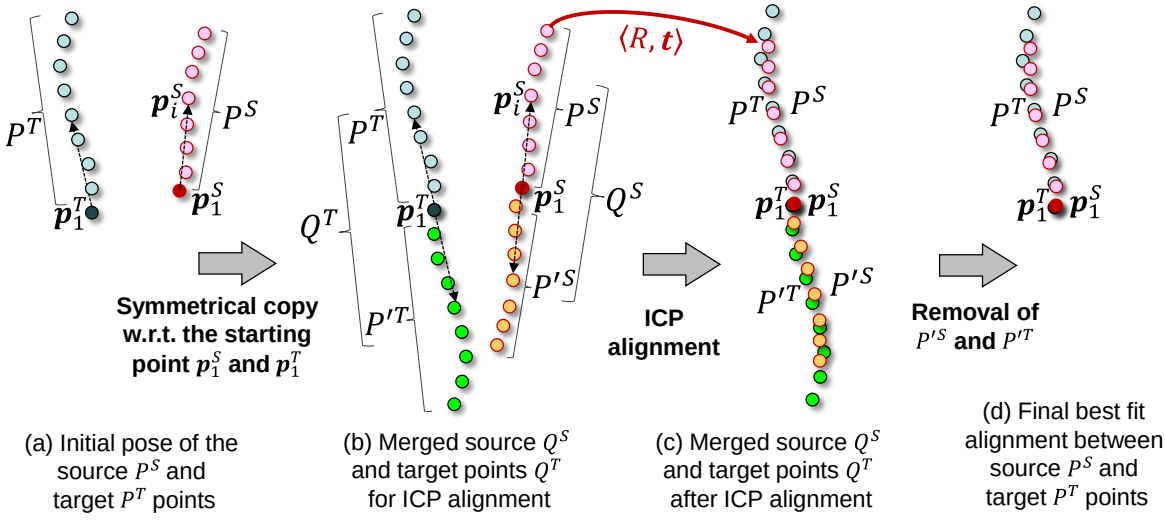

Figure 7: Process of the ICP-based best fit between the center points of two rods.

However, the original ICP always matches the centroids of P_c^i and P_c^j, and the fixation points to the sacrum of P_c^i and P_c^j do not coincide after the alignment. To avoid this, we have modified the original ICP-based alignment so that the fixation points on rods i and j, which are the starting points of evaluation intervals I_e^i and I_e^j, are perfectly matched. The evaluation interval I_e on each rod is determined by manually measuring the positions of fixing screws on the sacrum and thoracic spine T10 from the patient's radiograph after the surgery.

The proposed best fit alignment is performed as shown in Figure 7. First, the subsets of the sorted center points included in the evaluation intervals I_e^i and I_e^j are extracted as P_e^i and P_e^j from P_c^i and P_c^j. The points $\boldsymbol{p}_1^i \in P_e^i$, $\boldsymbol{p}_1^j \in P_e^j$ closest to the fixation points to their sacrum are selected as the starting points of P_e^i and P_e^j.

Second, between P_e^i and P_e^j, the center points with longer chord length are chosen as target points $P^T = \{\boldsymbol{p}_1^T, \cdots, \boldsymbol{p}_M^T\}$, and the ones with shorter chord length are chosen as source points $P^S = \{\boldsymbol{p}_1^S, \cdots, \boldsymbol{p}_N^S\}$ (Figure 7(a)). This chord length selection strategy is needed to make the closest distance evaluation between two-point clouds and the best fit alignment more accurate when using ICP.

Third, the points P^T and P^S are symmetrically copied using their starting points $\boldsymbol{p}_1^T$ and $\boldsymbol{p}_1^S$ to obtain the symmetric points P'^T and P'^S, and the merged target and source points $Q^T = P^T \cup P'^T$ and $Q^S = P^S \cup P'^S$ are created (Figure 7(b)). Fourth, the merged source points Q^S are best fitted with the merged target points Q^T using ICP.

As the centroids of both merged points Q^T and Q^S are starting points $\boldsymbol{p}_1^T$ and $\boldsymbol{p}_1^S$, this modified ICP algorithm can find the best fit alignment between the source and target points P^T and P^S so that

their starting points $\boldsymbol{p}_1^T$ and $\boldsymbol{p}_1^S$ are perfectly matched (Figure 7(c)). After the alignment, the optimum 3D transformation $\langle R, \boldsymbol{t} \rangle$ for the merged source points Q^S is obtained from this best fit alignment, where R is a 3 × 3 rotation matrix and $\boldsymbol{t}$ is a 3D translation vector for best fitting the points Q^S. Subsequently, we remove P'^S and P'^T from Q^S and Q^T to obtain the final best fit alignment of P^S to P^T (Figure 7(d))

Finally, we evaluate the RMS distance $D_{rms}^{i,j}$ between P_e^i and P_e^j in the evaluation intervals I_e^i and I_e^j from Equation (3.1).

$$D_{rms}^{i,j} = \sqrt{\frac{1}{|P^S|}\sum_{\boldsymbol{p}_k^S \in P^S} \left\| R\boldsymbol{p}_k^S + \boldsymbol{t} - \boldsymbol{p}_{c(k)}^T \right\|^2}, \tag{3.1}$$

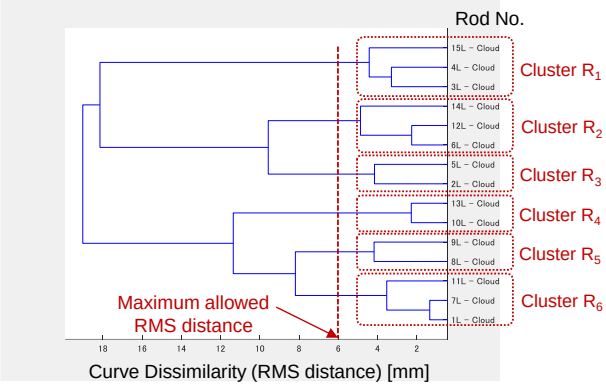

Figure 8: Dendrogram and the rod clusters corresponding to the maximum allowed distance.

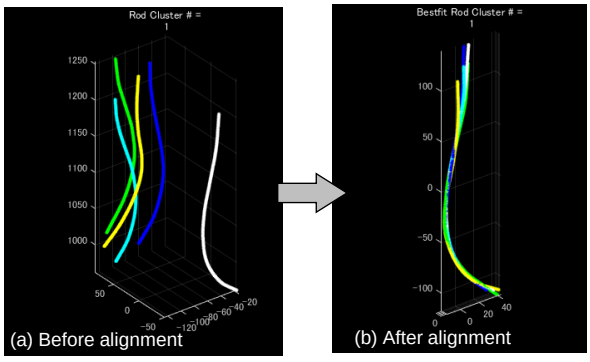

Figure 9: Best fit alignment of **c**enter points included in a cluster.

where $\boldsymbol{p}_{c(i)}^T$ is the point in target points P^T that is closest to $\boldsymbol{p}_i^S$ after the best fit. We adopt $D_{rms}^{i,j}$ as a measure of *curve dissimilarity* between the center points of rods i and j, and the dissimilarity evaluations are performed for all pairs of different rods (i,j) $(i,j \in R)$ in the CT-scanned rod set R.

3.4 Grouping of Similar-Shaped Rod Center Points by Hierarchical Cluster Analysis

The larger the number of standardized rods in the pre-bent rod set, the more it can be adapted to the individual differences in patients. However, this should be reduced as much as possible to save manufacturing costs.

Therefore, we perform a conventional hierarchical cluster analysis [26] where the curve dissimilarity between rod pairs, evaluated in Section 3.3, is used to mediate the analysis. From the dendrogram, we can analyze the relationship between the number of clusters that equal the number of standardized rods to be designed and the RMS distance among the existing rods belonging to one cluster (Figure 8). Finally, we partition the original rod set R into appropriate L rod clusters $R_1, R_2, \ldots\ldots, R_L$ $(R_1 \cup R_2 \cup \ldots\ldots \cup R_L = R)$ by setting a maximum RMS distance among center curves in one cluster allowed for the treatment (Figure 8). We selected this maximum allowed RMS distance around 5–6 mm, similar to our previous study on idiopathic scoliosis [17]. In the analysis, complete-linkage clustering is adopted as the linkage criteria.

Once the appropriate rod clusters $R_1, R_2, \ldots\ldots, R_L$ are identified, the center points of all rods included in each cluster are aligned to the best-fit positions and orientations, as shown in Figure 9, where the center points of the rod with the most extended cord length in the cluster are used as the reference position.

3.5 Derivation of the Center Curves of Standardized Rod Shapes by Least-Square Fitting

After the appropriate rod clusters are determined, the center curve of the standardized rod that best fits all center points of the rods included in a cluster is derived. Given a point cloud $Q = \{\boldsymbol{q}_1, \boldsymbol{q}_2, \boldsymbol{q}_3, \dots, \boldsymbol{q}_j, \dots., \boldsymbol{q}_K\}$ consisting of K aligned center points of rods included in a cluster R_i, we fit a K nth degree B-spline curve $\boldsymbol{S}(t)$ defined by Equation (3.2) with a uniform knot vector $\boldsymbol{T} = [t_0, t_1, t_2, \dots\dots, t_{m-1}, t_m]$ $(\forall i \neq j, t_i \neq t_j, |t_i - t_{i-1}| = const)$ to Q,

$$\boldsymbol{S}(t) = \sum_{i=0}^{m-n-1} \boldsymbol{P}_i N_{i,n+1}(t), \quad t \in [t_n, t_{m-n}], \tag{3.2}$$

where $\boldsymbol{P}_0, \boldsymbol{P}_1, \dots\dots., \boldsymbol{P}_{m-n-1}$ denote $(m-n)$ control points of the curve $\boldsymbol{S}(t)$, $N_{i,n+1}(t)$ is a normalized B-spline function of nth degree, and t is a parameter of the curve $\boldsymbol{S}(t)$

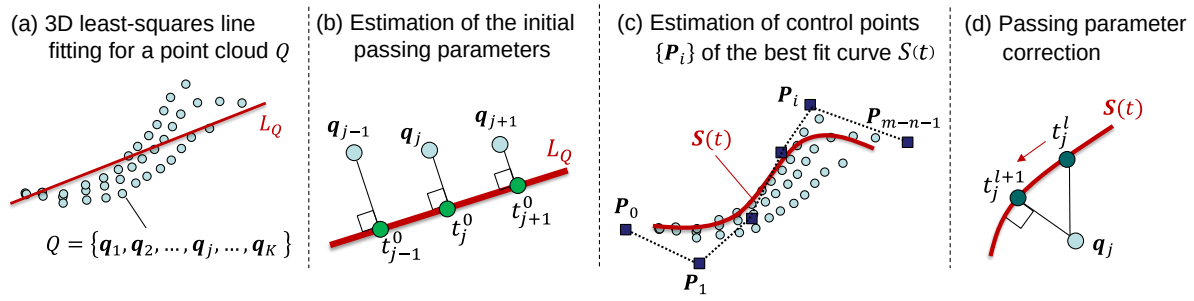

Figure 10: Best B-spline curve fit process to derive the center curve of the standardized rod shape of a rod cluster.

To find the optimum control point $\boldsymbol{P}_i$ of the curve $\boldsymbol{S}(t)$ that best fit Q, we use the following method of iterative least-square fitting and parameter improvement [24].

(1) A 3D least-squares line L_Q is fitted to the point cloud Q. We first perform the principal component analysis for Q and determine the equation of L_Q as $(u) = \boldsymbol{d}u + \overline{\boldsymbol{q}}$, where $\overline{\boldsymbol{q}}$ is a centroid position of Q and $\boldsymbol{d}$ is the normalized eigen vector of the covariance matrix for Q corresponding to the maximum eigen value of the matrix (Figure 10(a)).

(2) The initial values of the passing parameters $t^0_1, t^0_2, t^0_3, \dots\dots, t^0_{K-1}, t^0_K$ of the curve $\boldsymbol{S}(t)$ at points $\boldsymbol{q}_1, \boldsymbol{q}_2, \boldsymbol{q}_3, \dots, \boldsymbol{q}_j, \dots., \boldsymbol{q}_K (\in Q)$ are estimated from the projection of $\boldsymbol{q}_j$ on line L_Q as $t^0_j = (\boldsymbol{q}_j - \overline{\boldsymbol{q}}) \cdot \boldsymbol{d}$ (Figure 10(b)).

(3) As shown in Figure 10(c), the control point positions $\boldsymbol{P}_0, \boldsymbol{P}_1, \dots\dots., \boldsymbol{P}_{m-n-1}$ of the B-spline curve $\boldsymbol{S}(t)$ that fit Q with the passing parameters $t^0_1, t^0_2, t^0_3, \dots\dots, t^0_{K-1}, t^0_K$ are obtained by solving Equations (3.3–3.6).

$$P = (N^T N)^{-1} N^T Q, \tag{3.3}$$

$$\text{where} \quad P = \begin{bmatrix} P_{x,0} & P_{y,0} & P_{z,0} \\ \vdots & \vdots & \vdots \\ P_{x,i} & P_{y,i} & P_{z,i} \\ \vdots & \vdots & \vdots \\ P_{x,m-n-1} & P_{y,m-n-1} & b\ P_{z,m-n-1} \end{bmatrix}, \qquad \boldsymbol{P}_i = [P_{x,i},\ P_{y,i},\ P_{z,i}] \tag{3.4}$$

$$Q = \begin{bmatrix} q_{x,1} & q_{y,j} & q_{z,j} \\ \vdots & \vdots & \vdots \\ q_{x,j} & q_{y,j} & q_{z,j} \\ \vdots & \vdots & \vdots \\ q_{x,K} & q_{y,K} & q_{z,K} \end{bmatrix}, \qquad \boldsymbol{q}_j = [q_{x,j},\ q_{y,j},\ q_{z,j}] \tag{3.5}$$

$$N = \begin{bmatrix} N_{0,n+1}(t_1) & \cdots & N_{m-n-1,n+1}(t_1) \\ \vdots & \ddots & \vdots \\ N_{0,n+1}(t_K) & \cdots & N_{m-n-1,n+1}(t_K) \end{bmatrix} \tag{3.6}$$

(4) The passing parameter values $t_1^l, t_2^l, t_3^l, \ldots\ldots, t_{K-1}^l, t_K^l$ are updated to the new ones $t_1^{l+1}, t_2^{l+1}, t_3^{l+1}, \ldots\ldots, t_{K-1}^{l+1}, t_K^{l+1}$ by re-projection of center points $\boldsymbol{q}_1, \boldsymbol{q}_2, \boldsymbol{q}_3, \ldots, \boldsymbol{q}_j, \ldots., \boldsymbol{q}_K$ on the B-spline curve $\boldsymbol{S}(t)$ (Figure 10(d)). The updated parameter values can be obtained from Newton's method in Equations (3.7–3.9)

$$t^{l+1} = t^l - \frac{f(t^l)}{f'(t^l)} \tag{3.7}$$

$$f(t) = \boldsymbol{q}_j \cdot \sum_{i=0}^{m-n-1} \boldsymbol{P}_i N'_{i,n+1}(t) - \sum_{i=0}^{m-n-1} \boldsymbol{P}_i N_{i,n+1}(t) \cdot \sum_{i=0}^{m-n-1} \boldsymbol{P}_i N'_{i,n+1}(t) \tag{3.8}$$

$$\begin{aligned} f'(t) = \boldsymbol{q}_j \cdot \sum_{i=0}^{m-n-1} \boldsymbol{P}_i N''_{i,n+1}(t) - \sum_{i=0}^{m-n-1} \boldsymbol{P}_i N'_{i,n+1}(t) \cdot \sum_{i=0}^{m-n-1} \boldsymbol{P}_i N'_{i,n+1}(t) \\ - \sum_{i=0}^{m-n-1} \boldsymbol{P}_i N_{i,n+1}(t) \cdot \sum_{i=0}^{m-n-1} \boldsymbol{P}_i N''_{i,n+1}(t) \end{aligned} \tag{3.9}$$

(5) By repeating the least-square fitting of Equation (3.3) and re-projection of Equation (3.7) until the control point positions $\boldsymbol{P}_0, \boldsymbol{P}_1, \ldots\ldots, \boldsymbol{P}_{m-n-1}$ become stable, we can find the center curve of the standardized rod shape of a cluster $\boldsymbol{S}(t)$ that best fits the center points of similar-shaped rods as a B-spline curve. Usually, we can obtain stable positions of the control points by repeating Steps (3) and (4) above a few times.

After finding the best fit curve $\boldsymbol{S}(t)$, we finally generate the triangle mesh of the standardized rod shape by sweeping a circle with a standardized rod radius along the B-spline curve for all rod clusters. Of course, the geometry of the standardized rod surface is perfectly defined by the combination of its medial axis (B-spline curve) and radius. However, this rod surface reconstruction process is needed for two reasons. First, if the curvature of the medial axis is too large, its rod surface geometry might have a self-intersection that makes it difficult to manufacture. Therefore, we reconstruct the rod surfaces in order to check visually that the self-intersection does not occur. Second, we need to design and manufacture stamping die surfaces for mass production of pre-bent rods. Hence, we need to reconstruct the rod surfaces to design the die surface.

4 CASE STUDY

Twenty-six left and right spinal rods for 13 patients who underwent adult spinal deformity correction surgery at Dokkyo Medical University were measured by a medical CT scanner, and the shape similarity estimation between these rods was performed using the proposed method. We received informed consent from all patients before the study.

Figure 11 shows the reconstructed 26 rod surfaces represented by triangular meshes. We extracted the center points of each rod from the mesh using the method in Section 3.2, fitted a plane to these points in the least-square manner, and evaluated the distances of each center point from the best-fit plane. The distance distribution of the center points per rod is shown in the box plot of Figure 12. The figure clearly shows that spatial curves should represent the geometry of most spinal rods used for adult spinal deformity correction.

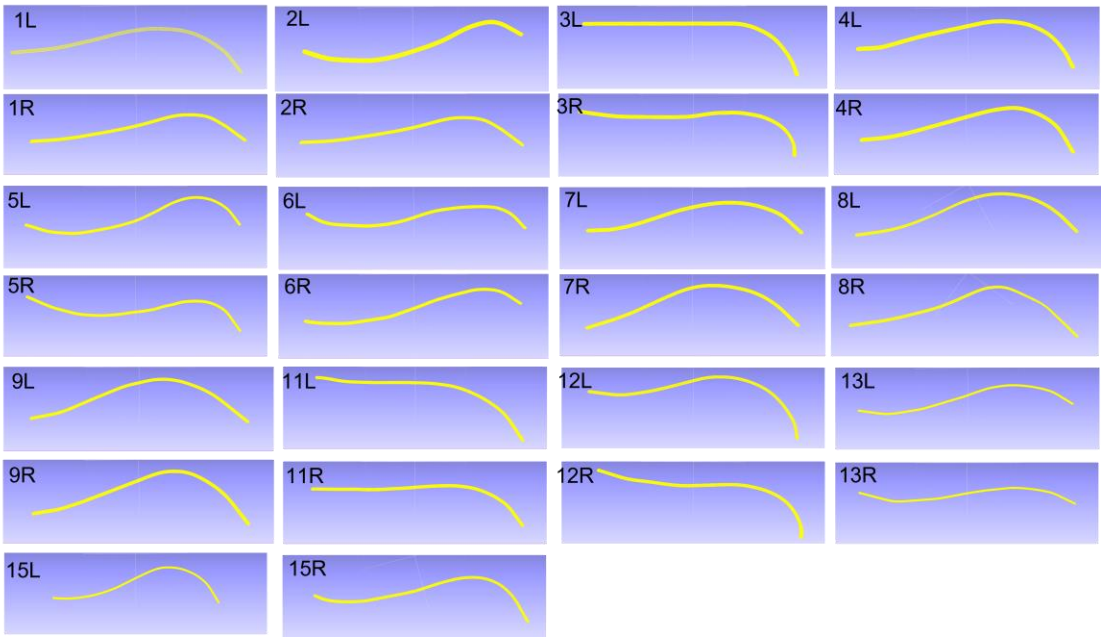

Figure 11: Twenty-six rod surfaces used for existing adult spinal deformity correction.

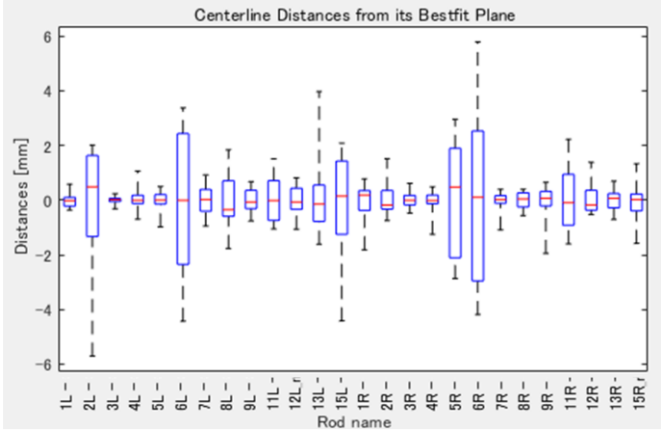

Figure 12: Distance distribution of the rod's center points from its best-fit plane.

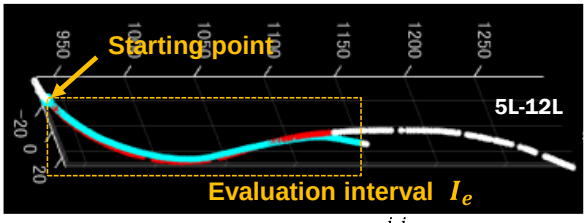

(a) Best fit of rod 5L and 12L, $D_{rms}^{i,j} = 1.66\ [mm]$

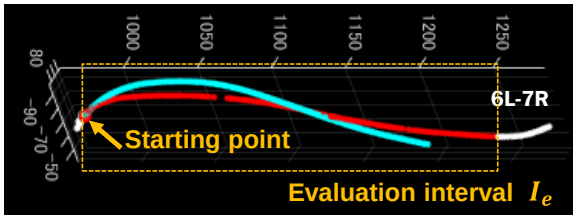

(b) Best fit of rod 6L and 7R, $D_{rms}^{i,j} = 8.39\ [mm]$

Figure 13: Examples of shape dissimilarity evaluation between two center points.

Figure 13 shows examples of shape dissimilarity evaluation between the center points of two rods. The evaluation is only limited to the evaluation interval I_e between the sacrum, the lumbar spine, and the thoracic spine T10. Figure 13 shows that the smaller the RMS distance $D_{rms}^{i,j}$, the more similar the rod shapes are, and that the distance $D_{rms}^{i,j}$ can work as a valid measure for the evaluation of rod shape dissimilarity.

Figure 14 shows a dendrogram of the hierarchical cluster analysis of 26 rod shapes using $D_{rms}^{i,j}$ as the measure of curve dissimilarity. From this dendrogram, many cases can be seen where the left and right rod shapes of different patients are highly similar, and it is considered that the pre-bent rods can be designed without distinguishing between the left and right rods. When the allowable RMS distance among the existing rod shapes in one cluster in the dendrogram was set to 6 mm, which is the tolerance allowed in normal surgery, five rod clusters were derived (Figure 14).

From these, we estimated that the rod shapes contained in four clusters (Clusters 1, 2, 4, and 5), including four or more rods, are highly versatile, and standardized pre-bent rods must be designed for these clusters. Meanwhile, the rod in Cluster 3, which contains only one rod, seems to have a peculiar shape, and since it is used infrequently, the need to design a pre-bent rod is low.

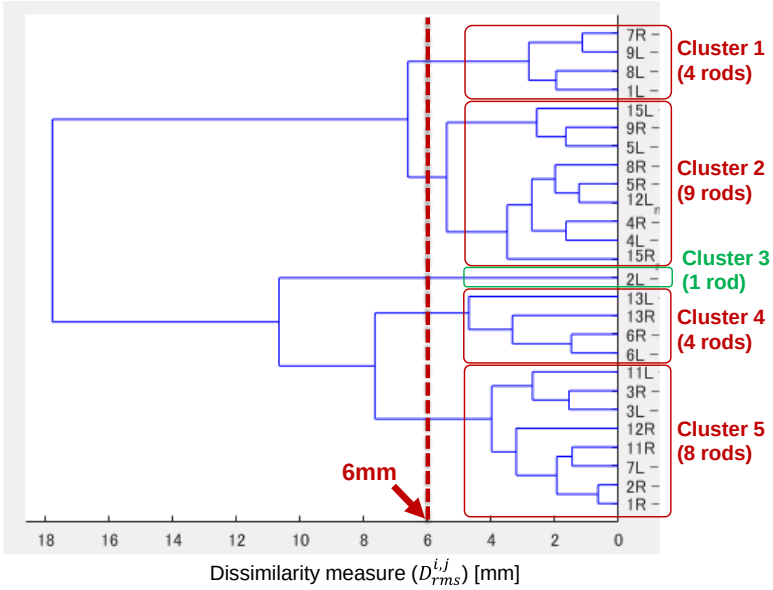

Figure 14: Dendrogram of the hierarchical cluster analysis, and derived rod clusters with the allowable RMS fit.

Finally, we derived the center curves of the four standardized rods corresponding to Clusters 1, 2, 4, and 5 within the evaluation interval I_e. From our preliminary tests, we selected a cubic B-spline curve with five control points ($n = 3, m = 8$) to stably derive the best-fit center curve of each cluster. Figure 15 shows the center points included in each cluster and the best-fit center curve of the standardized rod for the cluster.

We asked an orthodontic surgeon to evaluate the curves of the four standardized rods shown in Figure 15. The surgeon answered that the four curves could reproduce the rod curvature patterns frequently used in corrective surgeries for adult spinal deformity.

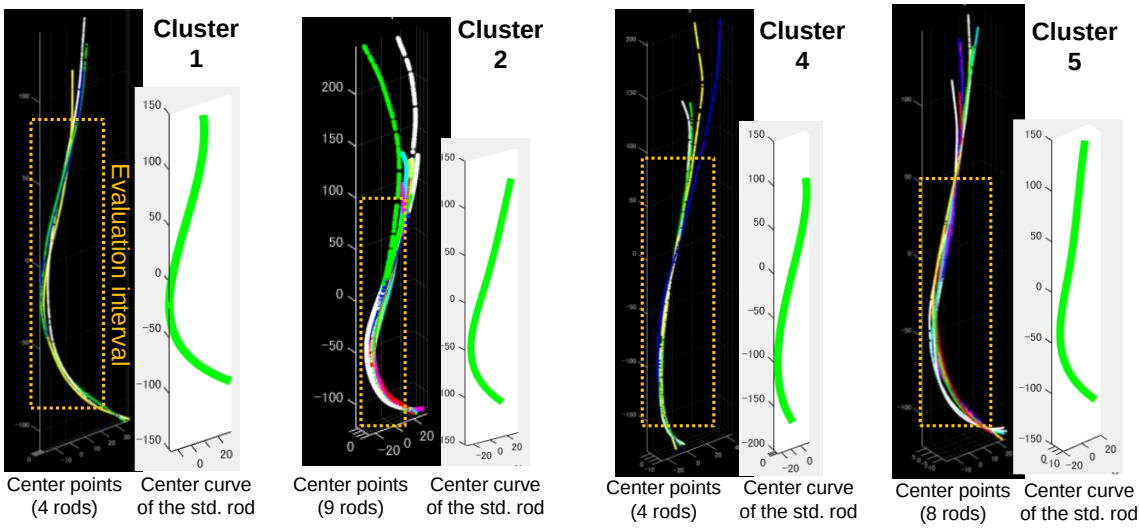

Figure 15: Center points of each cluster (multi-color), and derived center curves of the standardized pre-bent rods for the clusters (green).

This study has a limitation. We analyzed only a limited number of existing rod shapes. We previously analyzed pre-bent rod geometries from 46 adolescent idiopathic scoliosis patients [17]. In addition, clinical application of pre-bent rods with planar shapes designed for idiopathic scoliosis [17] has been recently reported [32]. The study [32] showed that patients with pre-bent rods had a significantly higher postoperative thoracic kyphosis than patients with conventional, manually bent rods. Moreover, the results in [32] suggested that a pre-bent rod can maintain its curvature, leading to better correction or maintenance of thoracic kyphosis after anatomical spinal correction surgery than the manually bent rod.

Since this paper is a preliminary study, a future study for adult spinal deformity patients should have as many cases as the previous study [17]. Furthermore, the clinical application of adult spinal deformity correction and its treatment efficacy should be provided to verify the proposed method. Although we do not intend to consider "perfectly normal anatomical correction" in adult spinal deformity surgery, notch-free pre-bent rods will reduce patients' burdens and the risk of rod breakage.

5 CONCLUSIONS

This work proposed a method to identify an optimal set of standardized pre-bent rods for correction surgeries of adult spinal deformity. The similarity evaluation among existing rod shapes using CT scan, medial axis extraction, and iterative closest point algorithm was described. Moreover, the derivation of standardized rod shapes using hierarchical cluster analysis and the best fit of the B-spline curve to each cluster were presented. The principle of the proposed method has been verified using CT scan measurements of 26 existing rods taken from 13 patients. Consequently, four different standardized rod shapes were derived using the proposed method. An orthodontic surgeon's preliminary evaluation of these rod shapes showed that the derived rod shapes could well represent the rod curvature patterns frequently used in corrective surgeries for adult spinal deformity.

In the future, we plan to verify the effectiveness of the proposed treatment method in 40 cases. Moreover, regarding manufacturing, a computer-aided method should be developed to support the design of complex stamping die surfaces for producing pre-bent rods with spatial curve shapes.

Ayane Soutome, http://orcid.org/0000-0001-8864-9995
Satoshi Kanai, http://orcid.org/0000-0003-3570-1782
Hiroaki Date, http://orcid.org/0000-0002-6189-2044
Terufumi Kokabu, https://orcid.org/0000-0002-2448-7402
Yuichiro Abe, http://orcid.org/0000-0001-8247-8128
Hiroshi Moridaira, http://orcid.org/0000-0002-9544-0636
Hiroshi Taneichi, https://orcid.org/0000-0003-2014-2922
Hideki Sudo, http://orcid.org/0000-0002-8635-4648

REFERENCES

[1] Abraham, C.; Cornillon, P.-A.; Matzner-Løber, E.; Molinari, N.: Unsupervised curve clustering using B-Splines, Scandinavian Journal of Statistics, 30(3), 2003, 581–595. http://www.jstor.org/stable/4616785
[2] Alliez, P.; de Verdire, E.-C.; Devillers, O.; Isenburg, M.: Isotropic surface remeshing, Proc. 2003 Shape Modeling International, 2003, 49-58. https://doi.org/10.1109/SMI.2003.1199601
[3] Andreopoulos, A.; Tsotsos, J. K.: Efficient and generalizable statistical models of shape and appearance for analysis of cardiac MRI, Medical Image Analysis, 12(3), 2008, 335-357. https://doi.org/10.1016/j.media.2007.12.003
[4] Besl, P.-J.; McKay, N.-D.: A method for registration of 3-D shapes, IEEE Transactions on Pattern Analysis and Machine Intelligence, 14(2), 1992, 239-256. https://doi.org/10.1109/34.121791
[5] Cardone, A.; Gupta, S.-K.; Karnik, M.: A survey of shape similarity assessment algorithms for product design and manufacturing applications, ASME. J. Comput. Inf. Sci. Eng., 3(2), 2003, 109–118. https://doi.org/10.1115/1.1577356
[6] Cheam, A. S.-M.; Fredette, M.: On the importance of similarity characteristics of curve clustering and its applications, Pattern Recognition Letters, 135, 2020, 360-367. https://doi.org/10.1016/j.patrec.2020.04.024
[7] Chudova, D.; Gaffney, S.; Mjolsness, E.; Smyth, P.: Translation-invariant mixture models for curve clustering, Proceedings of the ninth ACM SIGKDD international conference on Knowledge discovery and data mining, 2003, 79–88. https://doi.org/10.1145/956750.956763
[8] Dyke, R.M.; Lai, Y.K.; Rosin, P.L.; Tam, G.K.L.: Non-rigid registration under anisotropic deformations, Computer Aided Geometric Design, 71, 2019, 142-156. https://doi.org/10.1016/j.cagd.2019.04.014
[9] Eisenberger, M.; Lähner, Z.; Cremers, D.: Divergence-Free shape correspondence by deformation, Computer Graphics Forum, 38(5), 2019, 1-12. https://doi.org/10.1111/cgf.13785
[10] Engelborghs, K.; Kaimal, V.: Finding the best fit, Orthopedic Design & Technology Magazine, May/June, May 18th, 2012. https://www.odtmag.com/contents/view_features/2012-05-18/finding-the-best-fit/
[11] Fu, J.; Joshi, S.-B.; Simpson, T.-W.: Shape differentiation of freeform surfaces using a similarity measure based on an integral of Gaussian curvature, Computer-Aided Design, 40(3), 2008, 311-323. https://doi.org/10.1016/j.cad.2007.11.006
[12] Guo, B.; Hu, J.; Wu, F.; Peng, Q.: Automatic layout of 2D free-form shapes based on geometric similarity feature searching and fuzzy matching, Journal of Manufacturing Systems, 56, 2020, 37-49. https://doi.org/10.1016/j.jmsy.2020.04.019
[13] Han, R.; Uneri, A.; De Silva, T.; Ketcha, M.; Goerres, J.; Vogt, S.; Kleinszig, G.; Osgood, G.; Siewerdsen, J. H.: Atlas-based automatic planning and 3D-2D fluoroscopic guidance in pelvic trauma surgery, Physics in Medicine & Biology, 64(9), 2019, 095022. https://doi.org/10.1088/1361-6560/ab1456
[14] Heimann, T.; Meinzer, H.-P.: Statistical shape models for 3D medical image segmentation: A review, Medical Image Analysis, 13(4), 2009, 543-563. https://doi.org/10.1016/j.media.2009.05.004

[15] Iyer, N.; Jayanti, S.; Lou, K.; Kalyanaraman, Y.; Ramani, K.: Three-dimensional shape searching: state-of-the-art review and future trends, Computer-Aided Design, 37(5), 2005, 509-530. https://doi.org/10.1016/j.cad.2004.07.002
[16] Jacques, J.; Preda, C.: Functional data clustering: a survey, Adv Data Anal Classif, 8, 2014, 231–255. https://doi.org/10.1007/s11634-013-0158-y
[17] Kokabu, T.; Kanai, S.; Abe, Y.; Iwasaki, N.; Sudo, H.: Identification of optimized rod shapes to guide anatomical spinal reconstruction for adolescent thoracic idiopathic scoliosis, Journal of Orthopaedic Research, 36(12), 2018, 3219-3224. https://doi.org/10.1002/jor.24118
[18] Kuragano, T.; Yamaguchi, A.: Curve shape modification and similarity evaluation, 2006 International Conference on Computational Intelligence for Modelling Control and Automation and International Conference on Intelligent Agents Web Technologies and International Commerce (CIMCA'06), 2006, 227-227. https://doi.org/10.1109/CIMCA.2006.78
[19] Lee, D.-J.; Antani, S.; Rodney Long, L.: Similarity measurement using polygon curve representation and Fourier descriptors for shape-based vertebral image retrieval, Proc. SPIE 5032, Medical Imaging 2003: Image Processing, 2003. https://doi.org/10.1117/12.481912
[20] Lindsey, C.; Deviren, V.; Xu, Z.; Yeh, R.F.; Puttlitz, C.: The effects of rod contouring on spinal construct fatigue strength, Spine, 31(15), 2006, 1680-1687. https://doi.org/10.1097/01.brs.0000224177.97846.00
[21] Liu, X.; Yang, M. C.-K.: Simultaneous curve registration and clustering for functional data, Computational Statistics and Data Analysis, 53(4), 2009, 1361–1376. https://doi.org/10.1016/j.csda.2008.11.019
[22] Newton, P.O.; Yaszay, B.; Upasani, V.V.; Pawelek, J.B.; Bastrom, T.P.; Lenke, L.G.; Lowe, T.; Crawford, A.; Betz, R.; Lonner, B.; Harms Study Group: Preservation of thoracic kyphosis is critical to maintain lumbar lordosis in the surgical treatment of adolescent idiopathic scoliosis, Spine, 35(14), 2010, 1365-1370. https://doi.org/10.1097/BRS.0b013e3181dccd63
[23] Parent, S.; Shen, J.: Anterior vertebral body growth-modulation tethering in idiopathic scoliosis: Surgical Technique, Journal of the American Academy of Orthopaedic Surgeons, 28(17), 2020, 693-699. https://doi.org/10.5435/JAAOS-D-19-00849
[24] Plass, M; Stone, M.: Curve-fitting with piecewise parametric cubics, SIGGRAPH Comput. Graph., 17(3), 1983, 229–239. https://doi.org/10.1145/964967.801153
[25] Ramanathan, M.: Matching of shapes bound by freeform curves, Computer-aided Design and Applications, 9(2), 2012, 133-146. https://doi.org/10.3722/cadaps.2012.133-146
[26] Rokach, L.; Maimon, O.: Clustering Methods, In: Maimon, O., Rokach, L. (eds) Data Mining and Knowledge Discovery Handbook, Springer, Boston, MA, 2005. https://doi.org/10.1007/0-387-25465-X_15
[27] Sahillioğlu, Y.: Recent advances in shape correspondence, The Visual Computer, 36, 2020, 1705–1721. https://doi.org/10.1007/s00371-019-01760-0
[28] Salmingo, R.A.; Tadano, S.; Abe, Y.; Ito, M.: Influence of implant rod curvature on sagittal correction of scoliosis deformity, The Spine Journal, 14(8), 2014, 1432-1439. https://doi.org/10.1016/j.spinee.2013.08.042
[29] Santini, S.; Jain, R.: Similarity measures, IEEE Transactions on Pattern Analysis and Machine Intelligence, 21(9), 1999, 871-883. https://doi.org/10.1109/34.790428
[30] Shi, X.; Cao, L.; Reed, M.P.; Rupp, J.D.; Hoff, C.N.; Hu, J.: A statistical human rib cage geometry model accounting for variations by age, sex, stature and body mass index, Journal of Biomechanics, 47(10), 2014, 2277-2285. https://doi.org/10.1016/j.jbiomech.2014.04.045
[31] Sudo, H.; Abe, Y.; Kokabu, T.; Kuroki, K.; Iwata, A.; Iwasaki, N.: Impact of multilevel facetectomy and rod curvature on anatomical spinal reconstruction in thoracic adolescent idiopathic scoliosis, Spine, 43(19), 2018, E1135-E1142. https://doi.org/10.1097/BRS.0000000000002628
[32] Sudo, H.; Tachi, H.; Kokabu, T.; Yamada, K.; Iwata, A.; Endo, T.; Takahata, M.; Abe, Y.; Iwasaki, N.: In vivo deformation of anatomically pre-bent rods in thoracic adolescent idiopathic scoliosis, Scientific Reports, 11, 2021, 12622. https://doi.org/10.1038/s41598-021-92187-y

[33] Surazhsky, T.; Elber, G.: Matching free-form surfaces, Computers & Graphics, 25(1), 2001, 3-12. https://doi.org/10.1016/S0097-8493(00)00103-5
[34] Tagliasacchi, A.; Alhashim, I.; Olson, M.; Zhang, H.: Mean curvature skeletons, Computer Graphics Forum, 31, 2012, 1735-1744. https://doi.org/10.1111/j.1467-8659.2012.03178.x
[35] Tao, X.; Prince, J. L.; Davatzikos, C.: Using a statistical shape model to extract sulcal curves on the outer cortex of the human brain, IEEE Transactions on Medical Imaging, 21(5), 2002, 513-524. https://doi.org/10.1109/TMI.2002.1009387
[36] Zhang, Y.; He, K.; Jiang, J.; Chen, Z.: Construction and optimization of orthopedic plates based on average bone model, Computer-aided Design and Applications, 18(2), 2020, 227-241. https://doi.org/10.14733/cadaps.2021.227-241
[37] Zhang, Z.: Iterative point matching for registration of free-form curves and surfaces, Int J Comput Vision, 13, 1994, 119–152. https://doi.org/10.1007/BF01427149